Journal of Physics: Conference Series

The impact of weather patterns on offshore wind power production

The impact of weather patterns on offshore wind power production

Bedassa R Cheneka[1], Simon J Watson [1] and Sukanta Basu [2]

[1] Faculty of Aerospace Engineering, Wind Energy Section, Delft University of Technology, Delft, The Netherlands

[2] Faculty of Civil Engineering and Geosciences, Delft University of Technology, Delft, The Netherlands

E-mail: b.r.cheneka@tudelft.nl

Abstract. Large-scale weather systems have the potential to modulate offshore wind energy production. The Northern European sea areas have recently seen a rapid increase in wind power capacity and thus there is a need to understand how different weather systems affect offshore production from the perspective of energy system integration. In this study, mean sea level pressure data from a new-generation reanalysis (ERA5) are utilised to classify synoptic systems into 30 different weather patterns using a self-organising map (SOM) approach. ERA5 wind speeds are then used in conjunction with a reference 8 MW wind turbine power curve to estimate wind power values at selected offshore sites. We assess how wind power output varies for different weather patterns, specifically, the impact on power production and power ramps.

Keywords: self-organizing map, spatio-temporal variability, wind power ramps

1. Introduction

European countries have been developing offshore wind farm fleets particularly in the North and Baltic sea areas. These regions of the seas are suitable for wind farms due to their shallow depth and favourable wind speeds. Indeed, offshore wind speeds are generally higher in magnitude and lower in variability than onshore. Despite the lack of terrain, offshore areas still experience a significant degree of spatio-temporal variability caused by large-scale weather patterns.

It is clear that at any given time and location, the prevailing weather pattern influences the magnitude and fluctuation of wind speed. Several studies have been conducted on how meteorological systems determine the magnitude of wind speeds in different regions of the world [1, 2, 3]. These studies found that there is a strong association between weather patterns and wind speed. For example, a westerly wind flow and a rise in pressure tendency leads to a strong fluctuation in wind speed magnitude over the North Sea [4]. High-pressure centers and ridge systems generally lead to underproduction of wind power and vice-versa for the weather patterns characterised by low-pressure centers and trough systems [1]. In addition, wind power production is influenced by mesoscale systems [5]. As the current share of electricity generated from offshore wind power is increasing over Europe [5, 6], it is important to quantify the influence of large-scale weather patterns on wind power generation. This characterisation benefits the planning and utilisation of wind power production. With this in mind, we have classified weather patterns in order to explore how these patterns influence offshore wind power production in Northern European sea areas both in its magnitude and variability.

Meteorological reanalysis data have been used for regions where there is a lack of public-domain data and/or in-situ meteorological data. Studies have used global reanalysis wind speed data to quantify the spatio-temporal variability of wind speed and wind power [5, 7, 8, 9, 10].
The main objectives of the research presented in this paper are to: (i) reduce large-scale complex weather systems into a discrete number of patterns; (ii) to quantify the seasonal and spatial variation of wind power at several Northern European offshore sites; (iii) determine the association of wind power production and extreme wind power ramps with different weather patterns.

2. Methodology

2.1. Weather patterns

There has been previous work to classify European weather patterns into different clusters to identify the most prominent large-scale synoptic systems. For example, mean sea level pressure (MSLP) and the 500 mb geopotential height, which show a contemporaneous spatial correlation [11], have been used in the past for identifying large-scale weather features and for clustering weather patterns [1, 12].

Different clustering techniques have been used to identify coherent weather patterns. For instance, principal component analysis (PCA) was used to identify seven distinct European weather patterns [1] and k-means clustering was used to identify 30 European weather patterns [12]. In the current study, we have chosen to use a self-organising map (SOM) [13, 14] due to its ability to cluster nonlinear patterns. As the input layer to the SOM, we use hourly ERA5 mean sea level pressure (MSLP) data vectors for the period 2003–2017 over Western Europe. ERA5 is the recent high resolution fifth generation of ECMWF's atmospheric reanalyses of the global climate (ERA5) [15] which provides data for a range of meteorological variables at a grid size resolution of 30 km. The output layer of the SOM is the weather patterns defined by a number of neurons. Each neuron is initialized either linearly or randomly, derived from the first principal components of the input data vectors [16]. In this study, we use linear initialization combined with a batch learning algorithm. The batch learning algorithm is chosen as we are dealing with a large dataset. A number of iterations are performed to minimize the distance between input data vectors and the weighting of the neurons. A Gaussian neighborhood function is used so that input data vectors close to the neurons have more weight. For similarity calculation between input data vectors and the neurons' weight, we use a Euclidean distance and two phases of training are performed. In the first phase, we use a broad radius of influence, i.e. 5, with 30 iteration epochs, and in the second phase, we consider a radius of influence of 1 with 50 iteration epochs. In the second phase, the learning iterates more until there is no change in the topological order of the input data vectors. Finally, the input data vectors are assigned to the best matching unit (BMU) neurons. Furthermore, we have calculated the topographic error (TE) and quantization error (QE) to measure the quality of the weather patterns [13, 14, 18] as given by Equation 1 and 2.

$$TE = \frac{1}{T}\sum_{t_i=1}^{T} d(X_p(t)) \tag{1}$$

$$QE(p) = \frac{1}{T}\sum_{t_i=1}^{T} |X_p(t) - W_p(t)| \tag{2}$$

Where $\mathrm{X}_p(t)$ is the sample data for the weather pattern (p) with length t; $\mathrm{W}_p(t)$ is the weight vector of the BMU corresponding to the $\mathrm{X}_p(t)$ input data vector; and $\mathrm{d}(\mathrm{X}_p(t)) = 1$ if the first and the second data sample, $\mathrm{X}_p(t)$ are not in the same cluster, otherwise, $\mathrm{d}(\mathrm{X}_p(t)) = 0$.
QE measures the average difference of the sample data in each cluster from its BMU weight vector. It assesses the homogeneity of data represented in each cluster, whereas TE measures

the perseverance of the topology. TE indicates the temporal data sample being not found in adjacent cluster. A small value of these two parameters implies that the input data vectors are well represented by their assigned cluster [17].
Generally, the number of SOM clusters are determined subjectively based on the purpose for which they are intended. In this study, we have generated 30 weather patterns in a similar manner to [12] which used k-means. The 30 weather patterns that are produced using a SOM are shown in Fig. 1. The seven distinct weather patterns identified by [1] can be seen within the 30 patterns, namely: European Blocking (P27 and P28), Scandinavian Blocking (P26), Atlantic trough (P21), Zonal trough (P6), Scandinavian trough (P19), and Atlantic ridge (P23). Also, more prominent European weather patterns such as the Northerly cold front (P18 and P24) and British Isles Low Pressure (P2 and P3) are identified. Moreover, weather patterns show a topological order that distinguish high pressure from low pressure. High pressure is located at the bottom of the figure whereas low pressure is at the top. Note that in our analysis, we found an areal average of TE 0.042 meaning that 4.2% of the input data vectors in the BMU were not adjacent to each other. The QE values were highest (8.14%) and lowest (4.26%) for the weather patterns P1 and P19, respectively. These values would suggest that the data vectors were satisfactorily clustered by the 30 patterns.

2.2. Wind power metrics
We consider the variation in power characteristics for 10 representative offshore sites and relate them to the cluster patterns defined above. These sites are denoted as S_1–S_{10} and are shown in Fig. 2 (middle and right). The nearest grid point from ERA5 is chosen to calculate the representative wind turbine power output at that site. Wind speed values (U) at 100 m height are extracted from the ERA5 database and are converted to wind power $P(t, j)$ for each hourly time step t and grid point j using an 8 MW reference turbine wind power curve [19] as shown in Fig. 2 (top).
Firstly, we calculate for each weather pattern i and grid point j, the average power $P_{av}(i, j)$ over the period 2003 – 2017:

$$P_{av}(i,j) = \frac{\sum_{t_i=1}^{n_i} P(t_i, j)}{n_i} \tag{3}$$

where the summation is over the n_i hourly power values which occur in that weather class. We also define a climatological mean wind power for each grid point over all weather patterns:

$$P_g(j) = \frac{\sum_{t=1}^{N} P(t, j)}{N} \tag{4}$$

where, for the $m = 30$ weather classes:

$$N = \sum_{i=1}^{m} n_i \tag{5}$$

We now define a number of statistics of interest. The normalised percentage power deviation (PN) for each weather pattern and grid point, $PN(i, j)$ is given by:

$$PN(i,j) = \left(\frac{P_{av}(i,j) - P_g(j)}{P_g(j)} \right) \times 100\% \tag{6}$$

The variance of these values over all patterns, $\sigma_P^2(j)$ is defined:

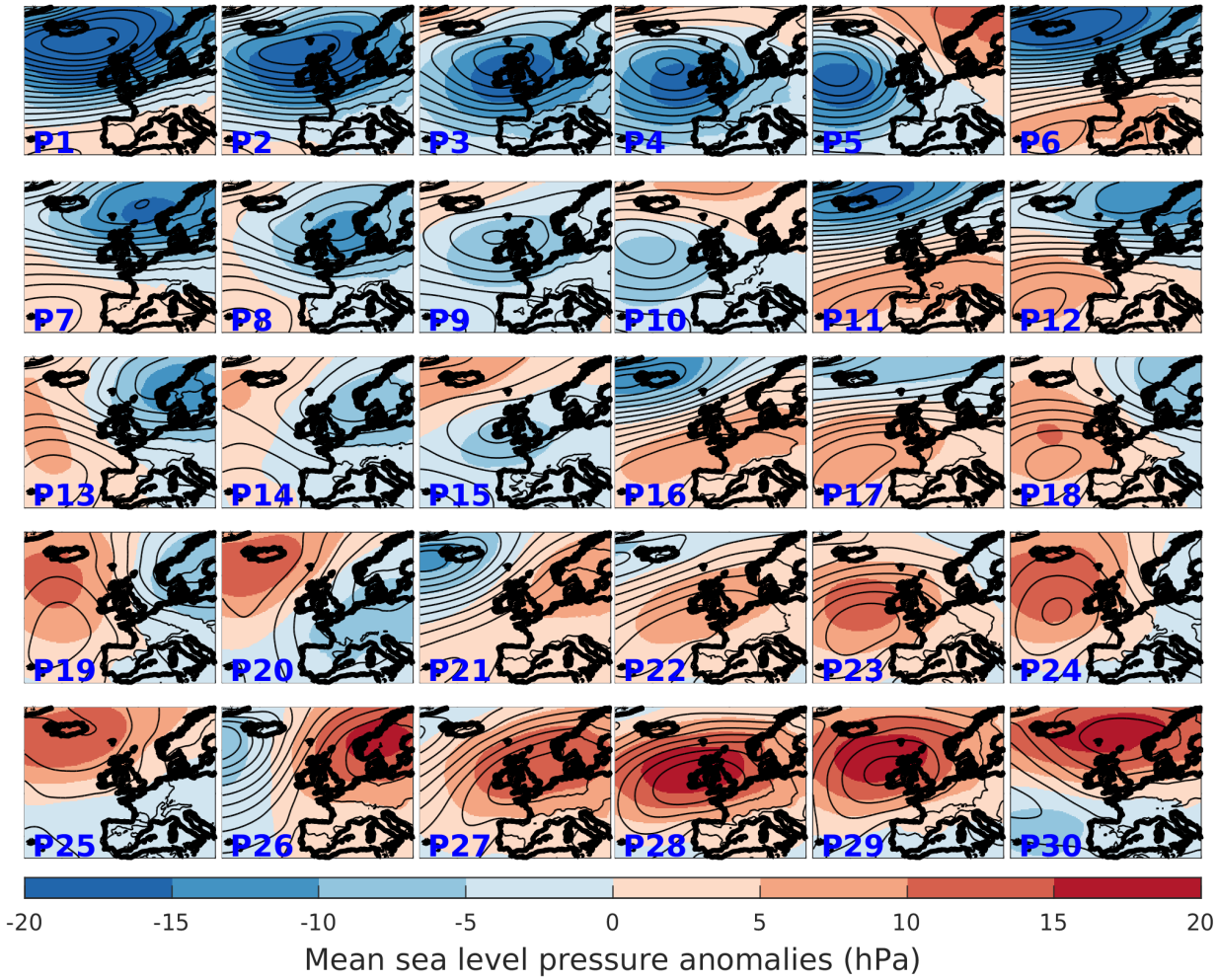

Figure 1 Weather patterns that are classified using a SOM. The contour lines shows the mean sea level pressure in intervals of 3hPa and the scale-colour is the mean sea level pressure anomalies (hPa).

$$\sigma_P^2(j) = \frac{\sum_{i=1}^{m} (PN(i,j) - PN_{av}(j))^2}{m-1} \tag{7}$$

where

$$PN_{av}(j) = \frac{\sum_{i=1}^{m} PN(i,j)}{m} \tag{8}$$

The hourly power ramp value, $R(t,j)$ at each time step is:

$$R(t,j) = P(t+1,j) - P(t,j) \tag{9}$$

For the entire time period 2003 – 2017, we derive the 95^{th} percentile ramp value, $R_{95}(i,j)$, from the ramp distribution at each grid point (i) broken down by weather pattern (j) which

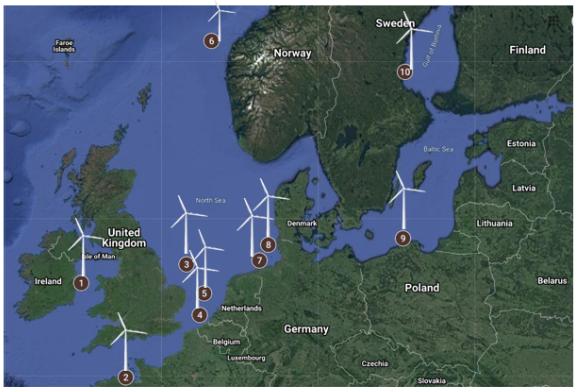

Sites (S)	Closest wind farms
S_1	Codling Wind Park
S_2	Saint-Brieuc
S_3	Hornsea Project One
S_4	Belwind Alstom Haliade
S_5	Borssele 1 and 2
S_6	Havsul I
S_7	Gode Wind 1 and 2
S_8	Horns Rev 3
S_9	Baltyk III - phase 2
S_{10}	Storgrundet

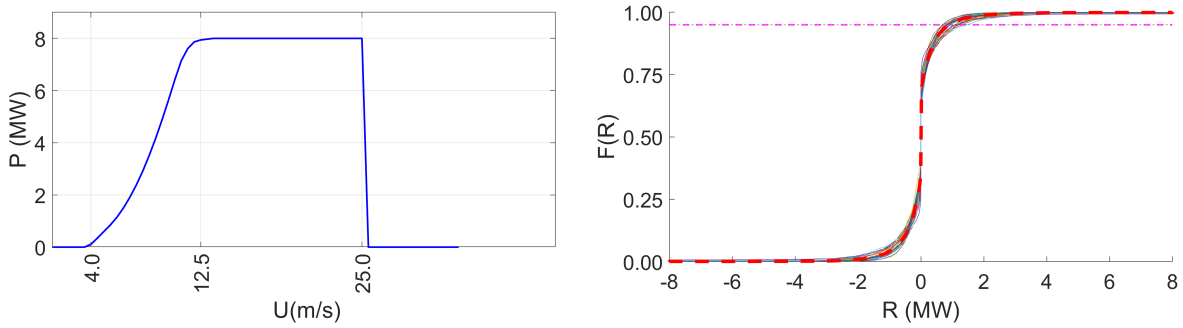

Figure 2 The sites used in this study (top panel), reference power curve for the 8 MW wind turbine (bottom-left panel). Power ramps distribution (bottom-right) for 2003 – 2017 (red dash line) and weather patterns. The dash magenta line is the 95% percentile used to identify extreme positive ramps.

we refer to as the extreme (positive) ramp value as shown in the Figure 2. We also derive $R_{g,95}(j)$ for each grid point over the entire period. From these we determine a value analogous to Eq. 6, namely the normalised percentage extreme ramp deviation for each pattern and grid point, $RN_{95}(i,j)$:

$$RN_{95}(i,j) = \left(\frac{R_{95}(i,j) - R_{g,95}(j)}{R_{g,95}(j)} \right) \times 100\% \tag{10}$$

Finally, we define the variance of these extreme power ramp values over all patterns, $\sigma_R^2(j)$:

$$\sigma_R^2(j) = \frac{\sum_{i=1}^{m} \left(RN_{95}(i,j) - R_{g,95}(j) \right)^2}{m-1} \tag{11}$$

3. Results

3.1. Spatial variation of wind power

Firstly, we examine the spatial variation in wind power from the hypothetical 8 MW turbine at each site over the entire period 2003 – 2017, averaged over all weather patterns. Fig. 3 (left) shows box-whisker plots based on 25^{th}, median and 75^{th} percentile of $P(t, j_S)$ are shown in blue, where j_S is the closest grid point to each of the 10 sites. Sites S_2 and S_{10} show the

lowest power production whereas S_4 and S_5 (which are farthest from the shore) show the highest power production. Sites S_1 and S_9 show very marked variation in seasonal output. As might be expected, all sites show the greatest wind power production during winter (DJF) and autumn (SON) and lowest during summer (JJA) and spring (MAM).
Fig. 3 (right) shows the 5^{th} percentile and 95^{th} percentile of the $R(t, j_S)$ values split by season. The strongest hourly wind power ramps are during spring and summer across most of the sites. There is significant seasonal variation in ramp magnitude. The sites which have the lowest mean power production, i.e. S_2, S_6, S_7, S_8 and S_{10}, show consistently high ramps across all seasons. The sites with higher mean output, i.e. S_4, S_5 and S_9 show significantly lower ramps during the winter months in particular. These findings are not so surprising as at the higher wind speed sites during winter, the turbine will be operating frequently above rated power thus reducing variability compared to lower wind speed sites where a much larger fraction of the time is spent between cut-in and rated wind speeds.

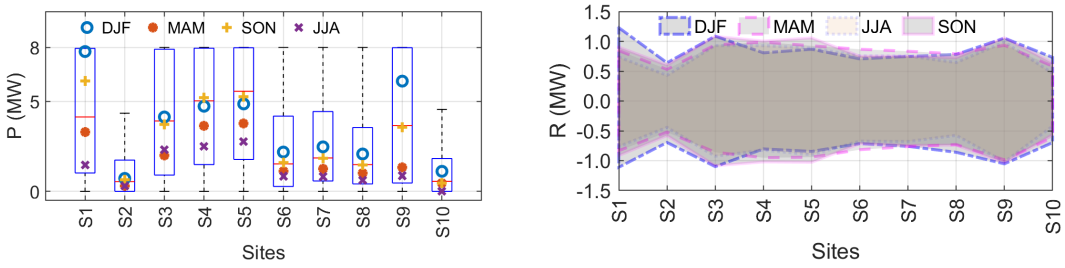

Figure 3 Seasonal and spatial variation of wind power (left) and wind power ramps (right) for an 8 MW wind power curve at the 10 selected sites. For the box-whisker plots of $P(t, j_S)$, the 25^{th} percentile, the median and 75^{th} percentile values are shown. For the power ramp values, $R(t, j_S)$, the shaded regions represent the 5^{th} and 95^{th} percentiles.

3.2. Association of wind power production with weather patterns

In this section, we examine the correlation between expected offshore wind power production and weather patterns, concentrating on four examples that show significant spatial variation: the British Isles low pressure (P2), the zonal trough (P6), the Scandinavian Blocking (P26) and the European Blocking (P27) synoptic systems. These four weather patterns were chosen as they represent a wide range of mean power production across the 10 sites. This can be seen in Fig. 4 (bottom-left) where the range of mean power production for all 30 patterns is superimposed as a shaded band on top of the mean power production for the four chosen weather patterns across the 10 sites. It can be seen from the contour plots in Fig. 4 that weather patterns P2 and P6 lead to higher than average wind power production over Northern Europe including the North Sea and to a lesser extent the Baltic Sea. By contrast, weather patterns P26 and P27 give rise to lower than average wind power production. This is broadly confirmed by the site specific values. When looking at the results for site S_9, it can be seen that there is rather less variation in the Baltic Sea for these weather patterns. Overall, low pressure systems contribute to higher than average wind power and vice-versa for high-pressure systems with some slight variation from site to site.

3.3. Correlation of wind power ramps with weather patterns

In this section, we investigate how extreme wind power ramps correlate with the four chosen weather patterns. Fig. 5 shows contour plots of $RN_{95}(i, j)$ as well as $R_{95}(i, j)$ and $RN_{95}(i, j)$ plotted for the 10 offshore sites and four weather patterns. In general, a higher magnitude of

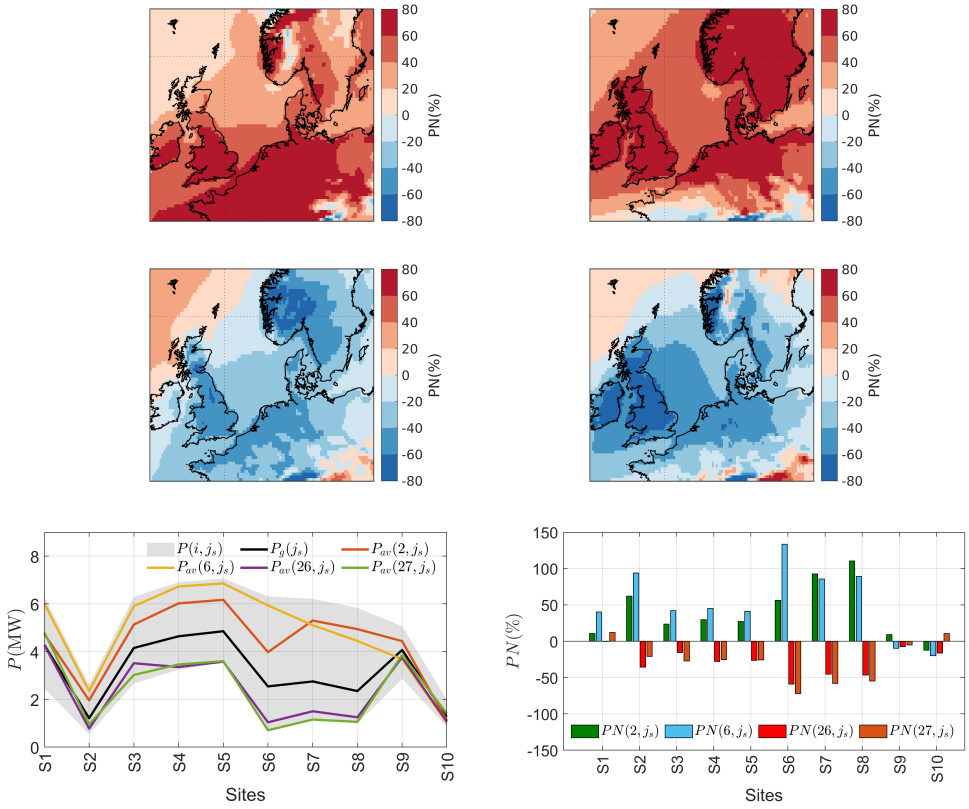

Figure 4 The association between specific weather patterns and wind power production: Contour plots of $PN(i,j)$ for (top-left) i=P2; (top-right) i=P6; (middle-left) i=P26; (middle-right) i=P27; (bottom-left) $P_{av}(i,j_S)$ for i= P2, P6, P26, P27, the mean over the entire period $P_g(j_S)$ and the shaded region ranges of wind power production:- upper bound is the maximum of $P(i,j_S)$ and lower bound is the minimum of $P(i,j_S)$ for the 10 sites as well as over the entire period ($P_g(j_S)$); and (bottom-right) the corresponding values of $PN(i,j_S)$.

extreme positive power ramps occurs during the prevailing low-pressure systems (P2 and P6) compared with high-pressure systems (P26 and P27).

It can be seen that there is a significant amount of spatial variation. In particular, for the low pressure weather patterns P2 and P6, there is a contrast between onshore and offshore where higher than average extreme ramps are seen in Northern Europe whereas in some of the near offshore regions, lower than average extreme ramps are observed. However, most of the study sites show slightly higher than average extreme ramps with the exceptions of the Baltic Sea sites, S_9 and S_{10}, particularly for pattern P6. In addition, the ramp magnitude for these two sites is lower than the other eight sites during this prevailing weather pattern. The Irish Sea site (S_9) shows the highest ramp magnitudes whereas the most southerly site, off the French coast, S_2 shows the lowest values in general. During patterns P26 and P27, lower than average extreme ramps are observed both onshore and offshore.

3.4. Trends over all 30 weather patterns and variance

Finally, we consider the different trends in power production, its variance and extreme power ramps at the 10 sites for all of the 30 weather patterns. These are summarised in Fig. 6. Those weather patterns which are associated with prevailing low pressure systems over the North European sea areas show higher than average wind power production, in particular, P1, P2, P3, P6, P7, P8, P11 and P12. Conversely, those weather patterns associated with high pressure

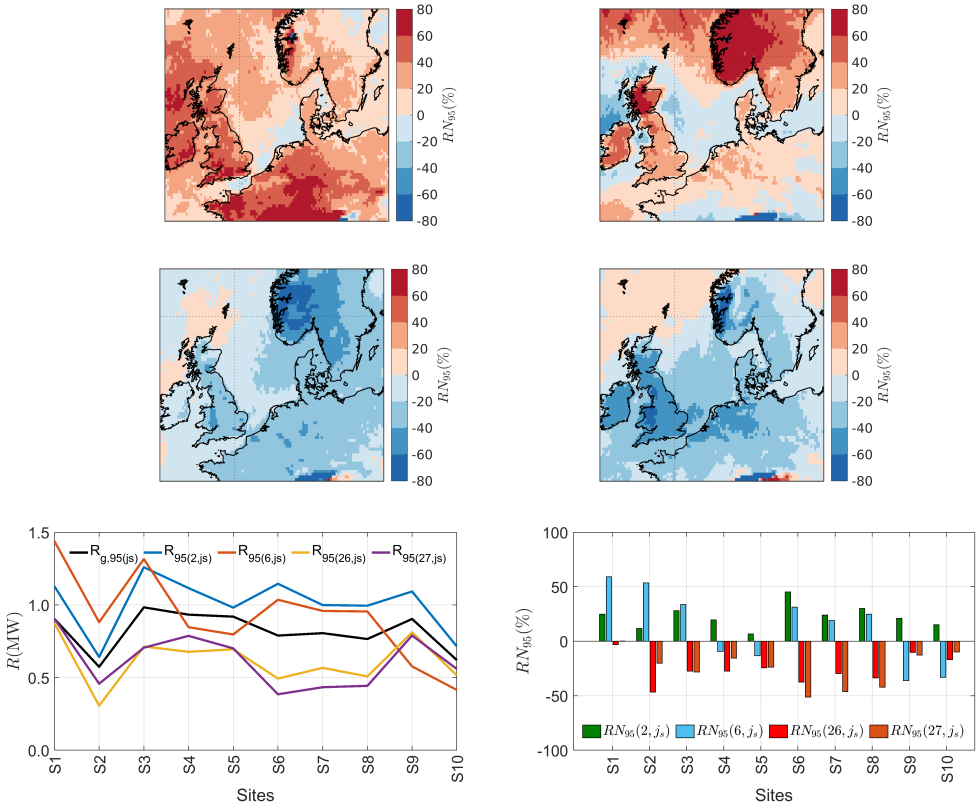

Figure 5 The association between specific weather patterns and extreme wind power ramps: Contour plots of $RN_{95}(i,j)$ for (top-left) i=P2; (top-right) i=P6; (middle-left) i=P26; (middle-right) i=P27; (bottom-left) $R_{95}(i,j_S)$ for i= P2, P6, P26 and P27 for the 10 sites as well as the mean over the entire period ($R_{g,95}(j_S)$); and (bottom-right) the corresponding values of $PN(i,j_S)$.

systems show lower than average production, especially P21-P30.

The trend for the magnitude of extreme wind power ramps is similar but not so pronounced. There are some differences between the sites as might be expected given their geographical spread. For example, site S6, the most northerly site, exhibits a large variation in average power across weather patterns; whereas site S9 (with a higher average wind power) in the Baltic shows little variation. Sites S3, S4 and S5 also show little variation. These sites with higher mean wind power and the patterns seen will have a relationship to the amount of time spent above rated wind speed, which will be greater for higher mean wind power (and thus higher mean wind speed) sites. This is confirmed by the fact that sites S4 and S5 show little variation in extreme wind ramps across the different classes. The exception to this is site S10 which is a low mean wind power site, where there is low variation of mean wind power and extreme power ramp magnitudes. The largest degree of variance in mean power and extreme power ramp magnitude is seen for the lowest mean wind power sites, S2, S6, S7 and S8. This is also consistent with the discussion above.

4. Conclusions

Spatial variation in large scale weather systems can cause significant variations in power generation and power ramps at offshore wind farm sites. We have presented a way of classifying weather systems into 30 different patterns which can be used to assess expected mean wind power and extreme ramp magnitude over a wide spatial area. Weather systems with prevailing

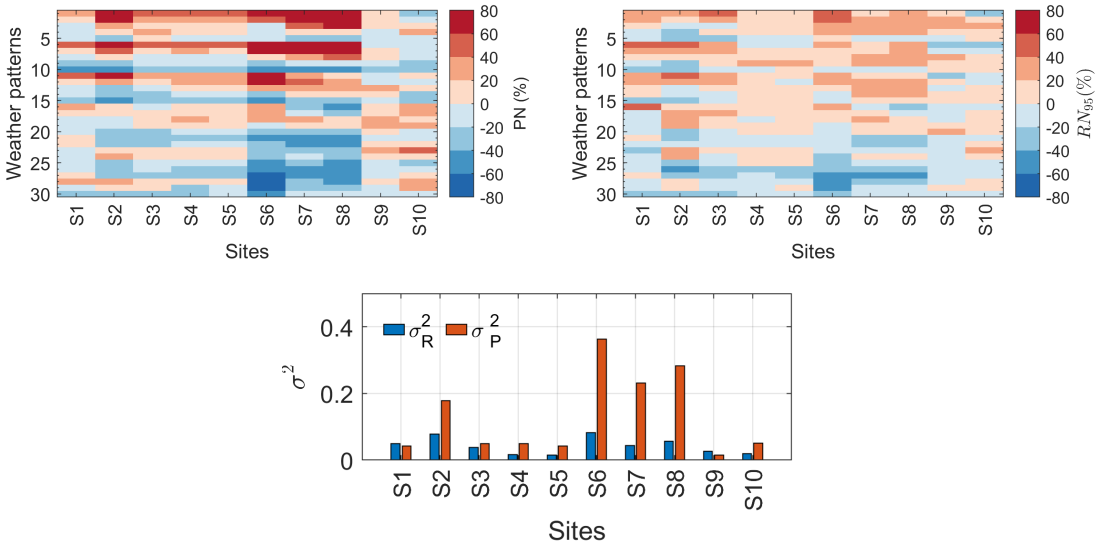

Figure 6 Variability in normalised power output, extreme ramp magnitude and their variance for the 30 weather patterns at the 10 offshore sites: (top-left) $PN(i, j_S)$; (top-right) $RN_{95}(i, j_S)$ and; (bottom) $\sigma^2_P(j_S)$ and $\sigma^2_R(j_S)$.

low pressure systems over Northern European sea areas tend to be associated with higher than average wind power output at offshore wind farm sites. Weather patterns dominated by high pressure systems show the opposite trend. Sites with higher mean wind power tend to show less variability across weather classes as wind turbines at these sites will be above rated power for a larger amount of the time. Reducing weather systems to a limited number of weather patterns which can be associated with expected mean power output or extreme ramp magnitudes could have a number of practical applications. For example, it could substantially reduce the computational effort required to predict future spatial and temporal trends in offshore wind power output under the influence of climate change which was a primary motivation for this work. The results could also be used in power system planning giving system and wind farm operators warning if a specific weather pattern is likely to the prevalent in a coming period. Furthermore, it could be used for operations and maintenance to assess likely patterns of loading of turbines in specific locations subject to particular weather patterns and for planning maintenance schedules. Also, it could be used to quantify forecast skill under different prevailing weather classes several days in advance. This could be important when assigning expected levels of uncertainty. In summary, classification into a relatively small number of patterns is of benefit to anyone involved with wind power who needs a convenient way to reduce the number of options they need to consider in the planning, maintenance or operation of wind farms. One important caveat to this work is that reanalysis data have limitations in reproducing local extreme wind speeds due to their finite spatial and temporal resolution. We would recommend further work incorporating in-situ data or the use of high-resolution mesoscale model downscaling such as NEWA (New European Wind Atlas) [20] and EURO-CORDEX (Coordinated Regional Downscaling Experiment) [21] to capture finer level extreme winds.

References

[1] Grams C M, Beerli R, Pfenninger S, Staffell I and Wernli H 2017 Balancing Europe's wind-power output through spatial deployment informed by weather regimes *Nature climate change* **7** 557–562
[2] Madonna E, Li C, Grams C M and Woollings T 2017 The link between eddy-driven jet variability and weather

regimes in the North Atlantic-European sector *Quarterly Journal of the Royal Meteorological Society* **143** 2960–2972
[3] Kempton W, Pimenta F M, Veron D E and Colle B A 2010 Electric power from offshore wind via synoptic-scale interconnection *Proceedings of the National Academy of Sciences* **107** 7240–7245
[4] Vincent C L, Pinson P and Giebela G 2011 Wind fluctuations over the North Sea *International Journal of Climatology* **31** 1584–1595
[5] González-Aparicio I, Monforti F, Volker P, Zucker A, Careri F, Huld T and Badger J 2017 Simulating European wind power generation applying statistical downscaling to reanalysis data *Applied Energy* **199** 155–168
[6] WindEurope 2020 Offshore wind in europe -key trends and statistics 2019. https://windeurope.org/
[7] Bett P E and Thornton H E 2016 The climatological relationships between wind and solar energy supply in Britain *Renewable Energy* **87** 96–110
[8] Cannon D J, Brayshaw D J, Methven J, Coker P J and Lenaghan D 2015 Using reanalysis data to quantify extreme wind power generation statistics: A 33 year case study in Great Britain *Renewable Energy* **75** 767–778
[9] Carvalho D, Rocha A, Gómez-Gesteira M and Santos C S 2014 Offshore wind energy resource simulation forced by different reanalyses: Comparison with observed data in the Iberian Peninsula *Applied Energy* **134** 57–64
[10] Staffell I and Pfenninger S 2016 Using bias-corrected reanalysis to simulate current and future wind power output *Energy* **114** 1224–1239
[11] Wallace J M and Gutzler D S 1981 Teleconnections in the geopotential height field during the Northern Hemisphere winter *Monthly Weather Review* **109** 784–812
[12] Neal R, Fereday D, Crocker R and Comer R E 2016 A flexible approach to defining weather patterns and their application in weather forecasting over Europe *Meteorological Applications* **23** 389–400
[13] Liu Y, Weisberg R H and Mooers C N 2006 Performance evaluation of the self-organizing map for feature extraction *Journal of Geophysical Research: Oceans* **111**
[14] Kohonen T 1998 The self-organizing map *Neurocomputing* **21** 1–6
[15] (2017): C C C S C 2020 ERA5 Fifth generation of ECMWF atmospheric reanalyses of the global climate *Copernicus Climate Change Service Climate Data Store (CDS)* https://cds.climate.copernicus.eu/
[16] Ciampi A and Lechevallier Y 2000 Clustering large, multi-level data sets: an approach based on kohonen self organizing maps *European Conference on Principles of Data Mining and Knowledge Discovery* (Springer) pp 353–358
[17] Le anh tu (october 14th 2019). improving feature map quality of som based on adjusting the neighborhood function [online first], intechopen, doi: 10.5772/intechopen.89233. available from: https://www.intechopen.com/online-first/improving-feature-map-quality-of-som-based-on-adjusting-the-neighborhood-function
[18] Kiviluoto K 1996 Topology preservation in self-organizing maps *Proceedings of International Conference on Neural Networks (ICNN'96)* vol 1 (IEEE) pp 294–299
[19] Desmond C, Murphy J, Blonk L and Haans W 2016 Description of an 8 mw reference wind turbine *Journal of Physics: Conference Series* vol 753 (IOP Publishing) p 092013
[20] Petersen E L, Troen I, Jørgensen H E and Mann J 2014 The new European wind atlas *Energy Bulletin* 34–39
[21] Jacob D, Petersen J, Eggert B, Alias A, Christensen O B, Bouwer L M, Braun A, Colette A, Déqué M, Georgievski G *et al.* 2014 EURO-CORDEX: new high-resolution climate change projections for European impact research *Regional environmental change* **14** 563–578